



# Evaluation of coupled finite element/meshfree method for a robust full-scale crashworthiness simulation of railway vehicles

Zhao Tang<sup>1</sup>, Feng Jia Liu<sup>1</sup>, Shi Hui Guo<sup>2</sup>, Jian Chang<sup>2</sup> and Jian Jun Zhang<sup>1,2</sup>

## Abstract

The crashworthiness of a railway vehicle relates to its passive safety performance. Due to mesh distortion and difficulty in controlling the hourglass energy, conventional finite element methods face great challenges in crashworthiness simulation of large-scale complex railway vehicle models. Meshfree methods such as element-free Galerkin method offer an alternative approach to overcome those limitations but have proved time-consuming. In this article, a coupled finite element/meshfree method is proposed to study the crashworthiness of railway vehicles. A representative scenario, in which the leading vehicle of a high-speed train impacts to a rigid wall, is simulated with the coupled finite element/element-free Galerkin method in LS-DYNA. We have compared the conventional finite element method and the coupled finite element/element-free Galerkin method with the simulation results of different levels of discretization. Our work showed that coupled finite element/element-free Galerkin method is a suitable alternative of finite element method to handle the nonlinear deformation in full-size railway vehicle crashworthiness simulation. The coupled method can reduce the hourglass energy in finite element simulation, to produce robust simulation.

## Keywords

Coupled finite element/meshfree method, crashworthiness, railway vehicles, crash simulation, mesh density sensitivity

Date received: 30 October 2015; accepted: 9 March 2016

Academic Editor: Neal Y Lii

## Introduction

With the increasing railway speed and traffic volumes, the crashworthiness performance of railway vehicles has become more important than ever to improve the passive safety of the vehicle in critical situation. During the past two decades, different methods have been used to evaluate the crashworthiness performance of railway vehicles. The most reliable way is full-scale experimental validation such as in Europe<sup>1</sup> and the United States.<sup>2–4</sup> However, full-scale real-vehicle impact experiment cannot be widely used in practice, because it is generally expensive, complex, time-consuming and unrepeatable. Recently, scaled tests of railway vehicle

collisions were used to investigate the energy absorption and dissipation pattern for various train sets.<sup>5</sup>

An alternative approach is numerical simulation, including multibody (MB) dynamics method and finite

<sup>1</sup>State Key Laboratory of Traction Power, Southwest Jiaotong University, Chengdu, China

<sup>2</sup>National Centre for Computer Animation, Bournemouth University, Poole, UK

## Corresponding author:

Zhao Tang, State Key Laboratory of Traction Power, Southwest Jiaotong University, 111 First Section, North of Second Ring Road, Chengdu, Sichuan 610031, China.

Email: tangzhao@swjtu.edu.cn



Creative Commons CC-BY: This article is distributed under the terms of the Creative Commons Attribution 3.0 License (<http://www.creativecommons.org/licenses/by/3.0/>) which permits any use, reproduction and distribution of the work without further permission provided the original work is attributed as specified on the SAGE and Open Access pages (<https://us.sagepub.com/en-us/nam/open-access-at-sage>).

element method (FEM). MB is generally used to simulate the dynamics of rigid bodies and can only provide limited accuracy for complex structures such as rail vehicles, while FEM can simulate the nonlinear large deformation in the case of vehicle crash, offering detailed analysis of different models and accurate simulation results.<sup>6–8</sup> However, the accuracy of the FEM strongly depends on the quality of the meshes.<sup>9</sup> In order to improve the accuracy of simulation results, conventional approach is to increase the mesh density of the input model. The FEM is computationally intensive in the case that a dense mesh is used. In addition, a higher mesh density does not necessarily guarantee the accurate results in crash simulation<sup>10</sup> due to the complexity and nonlinearity. Extra efforts are taken to create meshes at different levels of densities in order to achieve a balance between computational cost and simulation accuracy.

Another difficulty in rail vehicle crash simulation with FEM is how to reduce the hourglass energy. According to the ECE R66 standard,<sup>11,12</sup> the amount of non-physical energy (e.g. hourglass energy) should be less than 5% of total energy to ensure the reliability of simulation results. In FEM, the fully integrated elements do not produce hourglass energy for adopting full integration points. While their two disadvantages limit their application to full-scale crashworthiness simulation of railway vehicles. One is the low computational efficiency. The other is the shear locking. Fully integrated first-order elements generally suffer from the shear locking, leading to false simulation results. In order to improve the computational efficiency and to address the shear locking problem, the reduced integration element, especially reduced integration first-order element, is widely employed in the crashworthiness simulation of railway vehicles, which may introduce a considerable amount of hourglass energy. In LS-DYNA, improving the quality of the meshes can, to some extent, reduce the proportion of the hourglass energy. In practice, however, it is difficult to control the hourglass to a low level in full-scale crash simulation of railway vehicles. Moreover, hourglass control methods being available in LS-DYNA cannot work under all conditions. Previous experiences also show that it is not straightforward to control hourglass energy to a low level in large-scale rail vehicle crash FEM simulation involving nonlinear large deformation.<sup>10</sup>

An alternative to FEM is meshfree methods.<sup>13</sup> Without handling the element connectivity, a meshfree method is particularly effective in solving the problem of large deformations such as vehicle crash. However, a meshfree method needs much more computational costs than FEM, which limits its application to large-scale structures, such as trucks and railway vehicles. To improve the computational efficiency, a new coupled FEM/meshfree method (element-free Galerkin method

(EFGM)) has been proposed for automotive crashworthiness simulation recently.<sup>14–16</sup> To the best of our knowledge, using coupled FEM/EFGM for rail vehicle crashworthiness simulation has not yet been attempted.

In this article, we extend the application of the coupled FEM/meshfree method to the railway vehicle crashworthiness simulation. A representative scenario, in which a leading vehicle of a high-speed train impacts with a rigid wall, is simulated with the coupled FEM/EFGM in LS-DYNA. It shows that the coupled method can be applied to rail vehicle crashworthiness simulation with some additional computational cost. The comparison with conventional FEM shows the advantages of the proposed method in terms of adaptability and robustness.

## Introduction to coupled FEM/EFGM

Although FEMs have been proved to be effective to capture the nonlinear deformation<sup>17</sup> and widely used in rail vehicle crash simulation for many years, there still exist several challenges, such as numerical instability induced by mesh distortion and the requirements of complex pre-processing. Meshfree methods, such as EFGM, can address these challenges given its capability in dealing with large deformation and separation. However, computational expense is always the major bottleneck of the application of EFGM in large-scale simulation models, because it is generally much slower than FEMs (approximately six times in solving a numeral model at an equivalent scale<sup>18</sup>).

A coupled FEM/EFGM combines the advantages of both methods and allows modelling the severe deformation areas by solving large-scale simulation model with the EFGM<sup>16</sup> while effectively simulating the nonlinear deformation for other parts with FEMs. Early in 1995, the coupled FEM/EFGM was proposed by Belytschko et al.<sup>14</sup> But, it has not been used in solving large-scale complex structure crash simulation until recently, when an interface constraint coupling method has been developed and implemented into LS-DYNA version 971.<sup>15,16</sup>

As shown in Figure 1, the coupled FEM/EFGM divides the problem into two sub-domains: the FEM sub-domains  $\Omega_{\text{FEM}}$  where the finite element (FE) approximation is used and EFGM sub-domains  $\Omega_{\text{EFGM}}$  where meshfree approximation is employed.  $\Gamma_{\text{Interface}}$  refers to the interface between FEM sub-domains and EFGM sub-domain,  $\Gamma_{\text{Interface}} = \Omega_{\text{FEM}} \cap \Omega_{\text{EFGM}}$ . The main difference between FEM and EFGM is the shape function

$$\Psi(X) \neq \Phi(X) \quad (1)$$

where  $\Psi(X)$  is the shape function of EFGM;  $\Phi(X)$  is the shape function of FEM with Kronecker delta function property. To ensure the continuity of approximation across the interfaces, an interface constraint needs

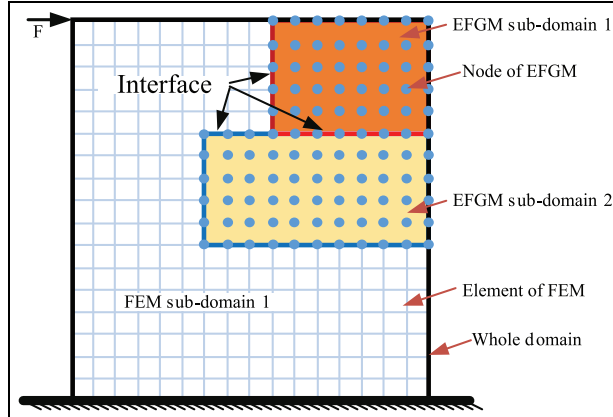


**Figure 1.** Coupled FEM/EFGM domain.

to be employed. The discrete approximation of the field variable is defined as follows<sup>16</sup>

$$u^h(X) = \begin{cases} \sum_{\substack{L=1 \\ x_L \in \Omega_{\text{FEM}}}}^{FP} \Phi_L^{[m]}(X) d_L, & \forall X \in \Omega_{\text{FEM}} \\ \sum_{\substack{I=1 \\ x_I \in \Omega_{\text{EFGM}}}}^{EP} \Psi_I^{[n]}(X; X - X_I) \left[ d_I - \sum_{\substack{J=1 \\ x_J \in \Gamma_{\text{Interface}}} \\ x_L \in \Omega_{\text{Interface}}}^{IP} \Phi_J^{[n]}(X_I) d_J \right] + \sum_{\substack{L=1 \\ x_L \in \Omega_{\text{Interface}}} \\ x_I \in \Omega_{\text{EFGM}}}^{IP} \Phi_L^{[m]}(X) d_L, & \forall X \in \Omega_{\text{EFGM}} \end{cases} \quad (2)$$

where  $\Phi_L^{[m]}$  is the  $m$ -order shape function of FEM;  $\Psi_I^{[n]}(X; X - X_I)$  is EFGM shape function constructed by moving least squares (MLS) approximation;  $\Psi_I^{[n]}(X)$  is the  $n$ -order shape function of coupled FEM/EFGM.  $FP$  is the number of the nodes in FEM sub-domains;  $EP$  is the total number of the nodes contained in EFGM sub-domains;  $IP$  is the total number of the nodes covered by the interfaces.  $d_L$  and  $d_I$  represent the displacement of the nodes located in sub-domain  $L$  and located in the interface  $I$ , respectively. In equation (2), if  $X$  is not contained in the influence domain of the interfaces,  $\Psi_I^{[n]}(X)$  will degenerate into the conventional MLS approximation. When the order of FEM interpolation  $m$  equals to the reproducing order  $n$ , we have

$$\bar{\Psi}_I(X) = 0, \text{ for all nodes} \\ \{I : \text{support } (\Psi_I) \cap \Gamma_{\text{Interface}} \neq \emptyset\} \text{ and } X \in \Gamma_{\text{Interface}} \quad (3)$$

Equation (3) is the interface constraint. When equation (3) is satisfied, equation (2) can be rewritten as

$$u^h(X) = \sum_{\substack{J=1 \\ x_J \in \Gamma_{\text{Interface}}} \\ i=1}^{IP} \Phi_J^{[m]}(X) d_{iJ} \quad \forall X \in \Gamma_{\text{Interface}}, \text{ for } i = 1, 2, 3. \quad (4)$$

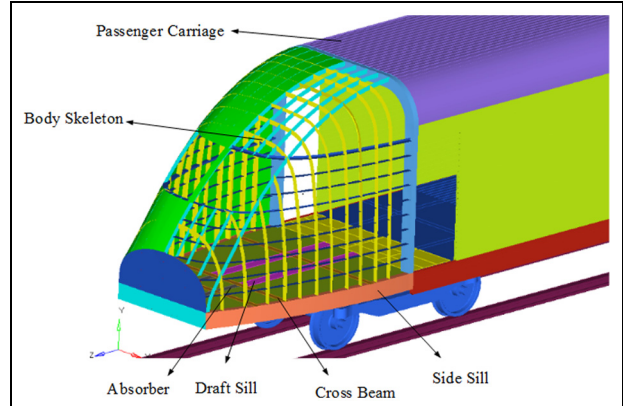


**Figure 2.** Simplified CAD model of a leading vehicle.

The shape functions of the interface degenerate into standard FEM shape function and satisfy the Kronecker delta function property. Thus, the conforming problem between FEMs and meshfree methods can be solved. More detailed description of coupled FEM/element-free Galerkin (EFG) theory can be found in Wang et al.<sup>15,16</sup>

## Modelling of a rail vehicle crash

In a train collision incident, the leading vehicle is required to absorb more energy than the intermediate ones. Therefore, in railway vehicle crashworthiness simulation, the crashworthiness of a leading vehicle is the critical research subject. This article focuses on the crash simulation of the leading vehicle of a high-speed train.

### Computer-aided design model

The popular symmetric model to reduce the amount of calculation is not used here because symmetric impact could lead to asymmetric deformations in thin-walled long-bar structures such as train.<sup>7</sup> Instead, a full-scale vehicle model is constructed by removing some components that have very little influence on the simulation results, including underframe equipment, weld parts, cowcatcher and so on from the complex computer-aided design (CAD) model. Some key components related to impact absorption, such as car body, energy absorber, draft sill, side sills and so on, are retained so that the model can yield reliable simulation of a real crash performance. The simplified CAD model of the leading vehicle is shown in Figure 2.

### FE model

Due to its good predictive capability in analysis of thick and thin structures,<sup>19</sup> we mainly use four-node three-

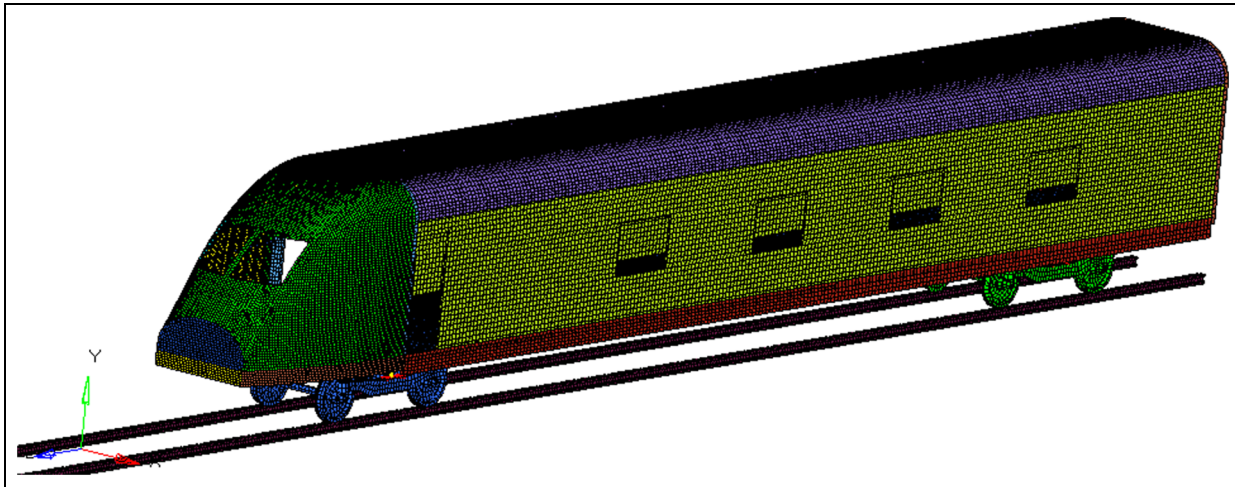


**Figure 3.** FE model of a leading vehicle.

**Table I.** Material properties.

Materials	Yield stress, $\sigma_y$ (MPa)	Young's modulus, $E$ (GPa)	Tangent modulus $E_{TAN}$ (MPa)	Poisson ratio
Q235	235	210	2100	0.34
A5083	150	66	1610	0.34
A7N01	245	70	1232	0.34

dimensional (3D) shell elements to construct the mesh of the car body, and the triangular element is also used in some irregular area. Assuming no derailment and override phenomena occur, the functions of the wheelsets and the bogies are only used to support the car body. Thus, the shell element with rigid material is suitable to model the wheelsets and bogies. The secondary suspension between bogies and car body is modelled by linear spring elements. And the lateral and the longitudinal stiffness of the spring elements are set to 158kN/m; the vertical stiffness of the spring elements is set to 280kN/m. To balance between the computational accuracy and efficiency, we set three different levels of mesh density for different components of the vehicle. An example of the FE model of a leading vehicle is shown in Figure 3.

### Material models

Due to the requirement of lightweight design, currently, almost all high-speed trains use aluminium alloy (A5083 or A7N01) to construct the major components. It is applied in car body, frame, energy absorber, centre sills, side sills and so on. In the connection parts, steel (Q235) is widely used to increase the structure strength. The material properties used in our study are described in Table 1.

The bilinear isotropic and kinematic hardening material model (MAT\_3 in LS-DYNA) is used when plastic deformation occurs. Considering the large

deformation in simulation, the hardening parameter  $\beta$  is set to 0 for kinematic hardening model. It generally uses two stages (elastic stage and plastic stage) to simulate the dynamic response

$$\begin{cases} E = \frac{d\sigma}{de}, & \sigma < \sigma_y \\ E_{TAN} = \frac{d\sigma}{de}, & \sigma > \sigma_y \end{cases} \quad (5)$$

where  $E$  denotes the Young's modulus in the elastic stage,  $E_{TAN}$  denotes the Tangent modulus in the plastic stage. The strain-stress curve of MAT\_3 is shown in Figure 4.

### Coupled FE/EFG modelling

For rail vehicle crash simulation, the collision usually creates large deformation in the frontend of the vehicle, particularly in the contact area. Figure 5 shows that in coupled FE/EFG modelling of rail vehicle crash, the traditional FE meshes located in the frontend of the rail vehicle are replaced by EFG models, including absorber, side-sill beam, floor plate and so on. The reason for this replacement is that these components will undergo severe load and produce nonlinear large deformation during the collision, causing potential risks of numerical instability. More importantly, these components are the major contributor to hourglass energy.

In LS-DYNA, there are three parameters for EFGM configuration. The first one is the kernel function. Available kernel function in LS-DYNA which includes cubic spline function, quadratic spline function and cubic spline function with circular disk. Here, we choose cubic spline function. The other two parameters, dilation parameters and normalized support size, control the size of influence domain which directly determines the simulation results.<sup>20</sup> Dilation parameter is used to specify the way of computing the size of basic influence domain based on the size of the adjacent integral element or the distance between nodes. The size of influence domain based on the former is larger than the latter. Normalized support size is to provide the smoothness and compact support properties on the construction of the EFGM shape functions.<sup>21</sup> In this

research, because the distribution of these nodes which use coupled FE/EFG algorithm is irregular, dilation parameters are based on the size of the adjacent integral element and the value of normalized support size is set to 1.01.

### Simulation scenario

As shown in Figure 6, the simulation scenario used in this study is a leading vehicle impacting with a rigid wall, which has been a representative scenario of rail vehicle crash simulation and widely used for crash-worthiness evaluation in railway industry. The initial velocity of the vehicle is 80 km/h, which damages the front-end structure of the leading vehicle. All degrees of freedom of the rigid wall and tracks are constrained. The surface contact between the vehicle and the wall as well as that between the wheelsets and the tracks is modelled with Coulomb's law of friction. Considering the train did not take any braking measures, the coefficient values of dynamic and static friction for the contact between the wheelsets and the tracks are all set to 0.1. The coefficient values of dynamic and static friction for other contacts are set to 0.15 and 0.2, respectively. The overall simulation is performed for 0.3 s, which is long enough to record the collision response.

### Results and discussion

In order to study the difference between FEM and coupled FEM/EFGM, we mesh the front-end structure of the leading car with different levels of mesh size, 20, 50 and 80 mm, respectively. The statistics of different mesh density models are listed in Table 2.

All three models with different levels of mesh density are all solved both by FEM and coupled FEM/EFGM and implemented on a computer with 3.33 GHz Intel(R) Xeon(R) CPU and 12 GB RAM.

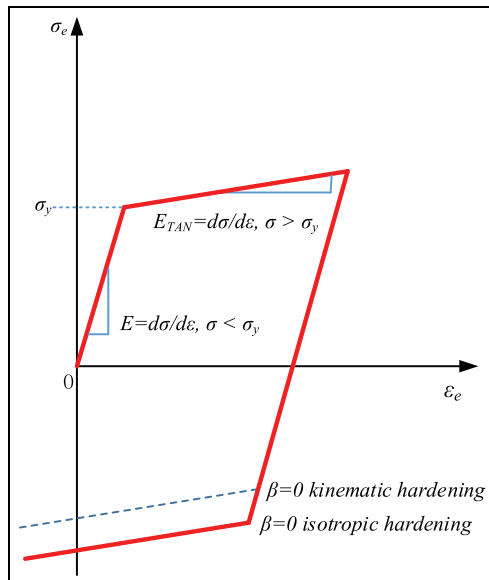


**Figure 4.** Stress–strain curve of MAT\_3 in LS-DYNA.

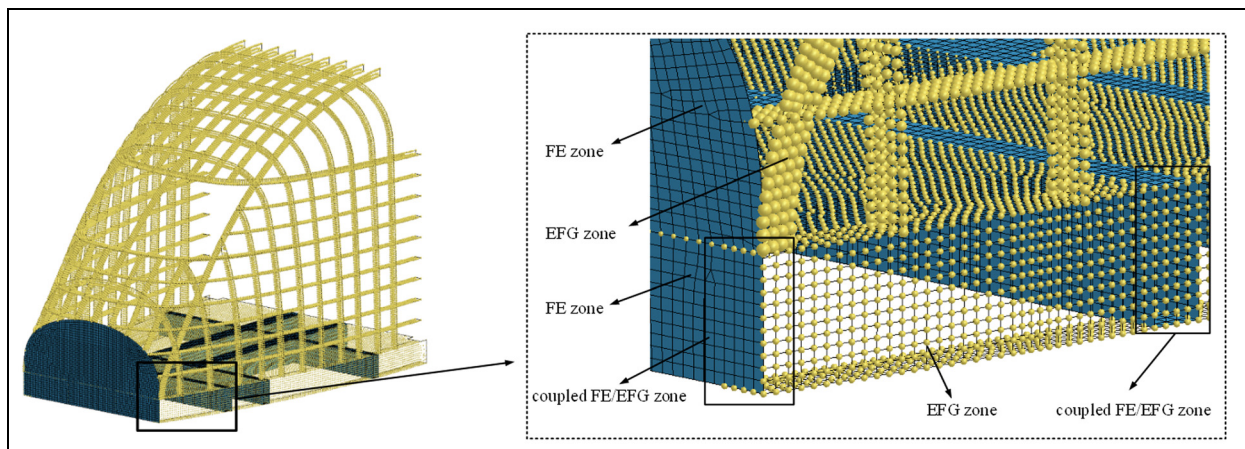


**Figure 5.** Coupled FE/EFG model of the front-end structure.

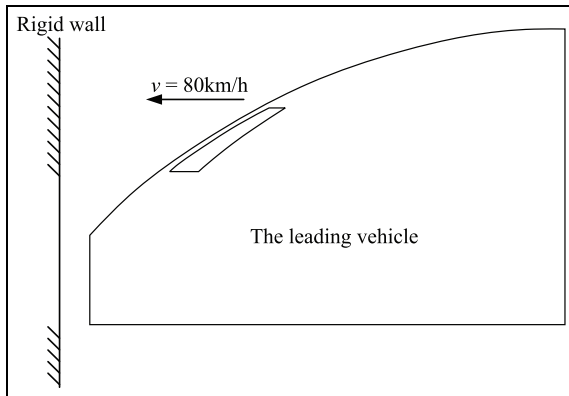


**Figure 6.** Simulation scenario.

### Simulation results

For simplicity, in this section, we only discuss the simulation results of case S1. The simulation results of other two cases will be used in section ‘Discussion’.

**Deformations.** A controlled progressive collapse of the front-end structure is critical for rail vehicle crashworthiness design to absorb energy. The deformation sequence of the front-end structure of a leading vehicle during the collision is shown in Figure 7. To display the deformation clearly, the second half of the leading vehicle is omitted. From the figure, the front side sill, absorber and front underframe had contacted the rigid wall and collapsed first, absorbing the most of the total energy. Afterwards, the cab begins to deform and absorbs the remaining energy.

**Total energy.** Total energy is a useful parameter for verifying the correctness of the simulation results of an explicit FE model. If the total energy is approximately constant, the overall error of the simulation result is usually less than 1%.<sup>12</sup> The internal energy, kinetic energy and total energy varying with time are shown in Figure 8.

As can be seen in Figure 8, the values of the initial kinetic energy in both cases are the same (8.25 MJ). During the first 10 ms, the kinetic energy decreases dramatically while the internal energy correspondingly increases, which is caused by the high collision velocity during this initial period. Afterwards, the kinetic energy decreases at a relatively slow rate until it is absorbed totally by the structural deformation and transformed into internal energy. The total energy of both methods is 8.25 MJ. After accomplishing the simulation, the mean total energy of both methods is 8.19 MJ and the error is 0.72%. So, it is evident that in both methods, the total energy is approximately constant, which is essential to confirm the correctness of the simulation

results. These results (both section ‘Deformations’ and ‘Total energy’) justify the application of the coupled FEM/EFGM to simulate the scenario of a railway vehicle crash.

### Discussion

**Computational efficiency.** Figure 9 shows the recorded computation time for the deferent mesh size using FEM and coupled FEM/EFGM, respectively. Obviously, the coupled FEM/EFGM has consumed more time than FEM in all three cases. But, it is worth noting that the value of mesh size 50 mm is only 10 h 41 min which is less than 12 h and is acceptable in real engineering application.

From Figure 9, in case S1, the computation time of FEM is 7 h 36 min, while the computation time of coupled FEM/EFGM is 30 h 47 min which is more than four times as much as FEM. But, in case S2, the computation time of coupled method is just about two times compared with FEM. In case S3, the computation time of the coupled FEM/EFGM is almost equal to the one of FEM, with a small fraction increase. The data demonstrated that mesh density has greater influence on the computation time of coupled FEM/EFGM than on FEM. Therefore, care should be taken when increasing the mesh density in coupled FEM/EFGM so that it does not lead to unacceptable computation time.

As shown in Figure 9, the coupled FEM/EFGM has also consumed more memories than FEM in three cases. In case S1, the memory consumption of FEM is 841 MB, approximately two-thirds the number of coupled FEM/EFGM, at 1223 MB, and the consumption of both methods is acceptable in real engineering application. With increasing in the mesh size, the memory consumption of coupled FEM/EFGM has reduced to 525 MB which is close to the consumption of FEM. In case S3, the memory consumption of both methods is almost the same. Thus, with the increasing in the mesh density, the memory consumption of coupled FEM/EFGM increased greater than that of FEM. Attentions should be paid to control the model’s mesh density to prevent the memory shortage.

**Underframe deformation modes.** Underframe is one of most important components in the leading rail vehicle crashworthiness simulation, because it undergoes large deformation when the collision occurs. The observation of the underframe deformation is one of the criteria to assess the reliability of a simulation result. According to the analysis method of a rail vehicle impacting with a rigid wall proposed by Xue et al.,<sup>7</sup> the underframe in our model should produce a deformation of bending downward in the predefined scenario due to friction force of contact area and the downward pitch moment

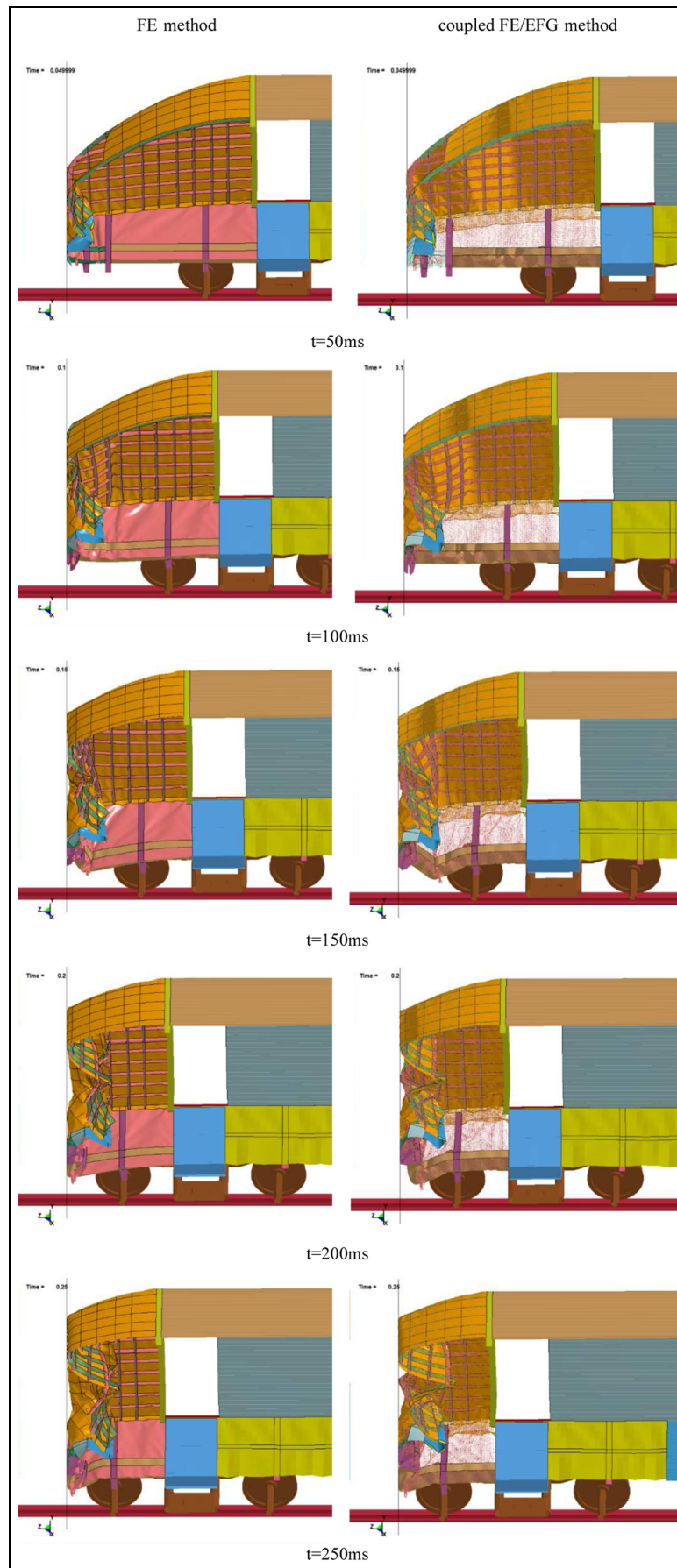


**Figure 7.** Deformation sequence of the front-end structure of a leading vehicle.

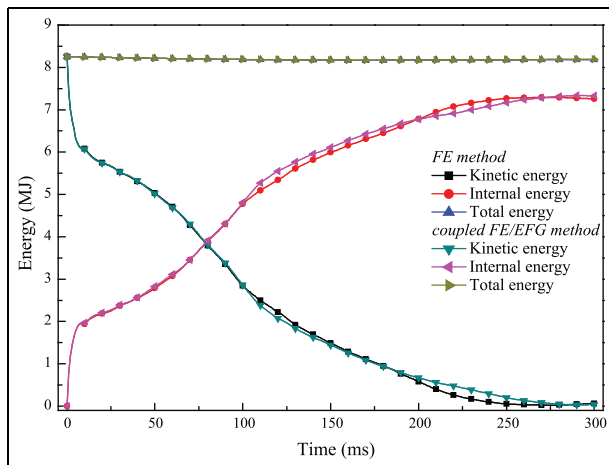


**Figure 8.** Internal energy, kinetic energy and total energy versus time.

**Table 2.** Statistics of different mesh density models.

Case	Mesh size (mm)	Elements	Nodes
S1	20	253,496	191,097
S2	50	172,043	110,970
S3	80	153,295	92,833

of the leading vehicle. The underframe deformations of three cases with both methods are shown in Figure 10.

As shown in Figure 10, in case S1, both methods have produced the expected deformation of bending

downward; in case S2, the coupled FEM/EFGM produces consistent deformation of bending downward as in case S1, while the one produced by FEM undergoes unexpected result of bending upward; in case S3, both methods produce the deformation of bending upward, which is not in accordance with the analysis framework of Xue et al.<sup>7</sup> It is worth noting that at the same level of mesh density (case S2), the coupled FEM/EFGM performs better than pure FEM. The coupled FEM/EFG can produce the deformation, which is consistent with the predicted results of higher density FE mesh (case S1). It indicates that compared to FEM, the coupled FEM/EFGM can produce reasonable simulation result using relatively coarse mesh model. This characteristic is helpful in improving the computation efficiency of coupled FEM/EFGM when applied to rail vehicle crashworthiness simulation. Namely, the coupled FEM/EFGM may allow using a mesh model of lower density, which reduces the computation time, while achieving the similar result as the FEM using a mesh model of higher density.

**Mesh density sensitivity.** The time series of energy for both FEM and coupled FEM/EFGM of different levels of mesh density are plotted in Figure 11.

At the initial stage of the crash, the internal energy curves of both methods increase faster in the case of lower mesh density, which means a finer mesh model dissipates kinetic energy into structure deformation at a slower rate than a coarser one. It is because the finer

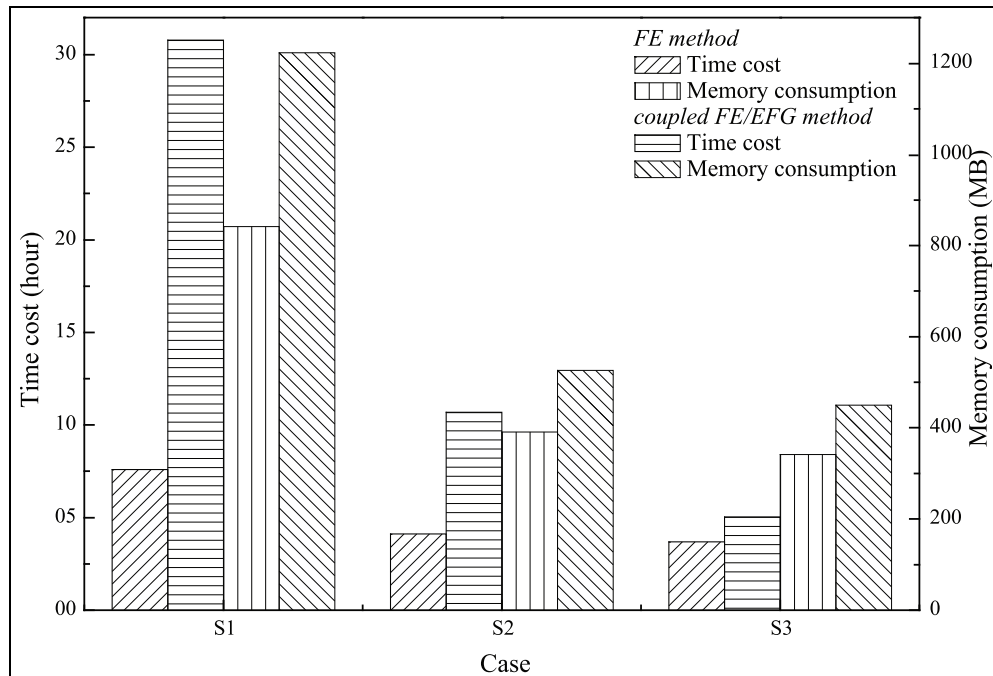


**Figure 9.** Computation consumption of two methods with different levels of mesh density.

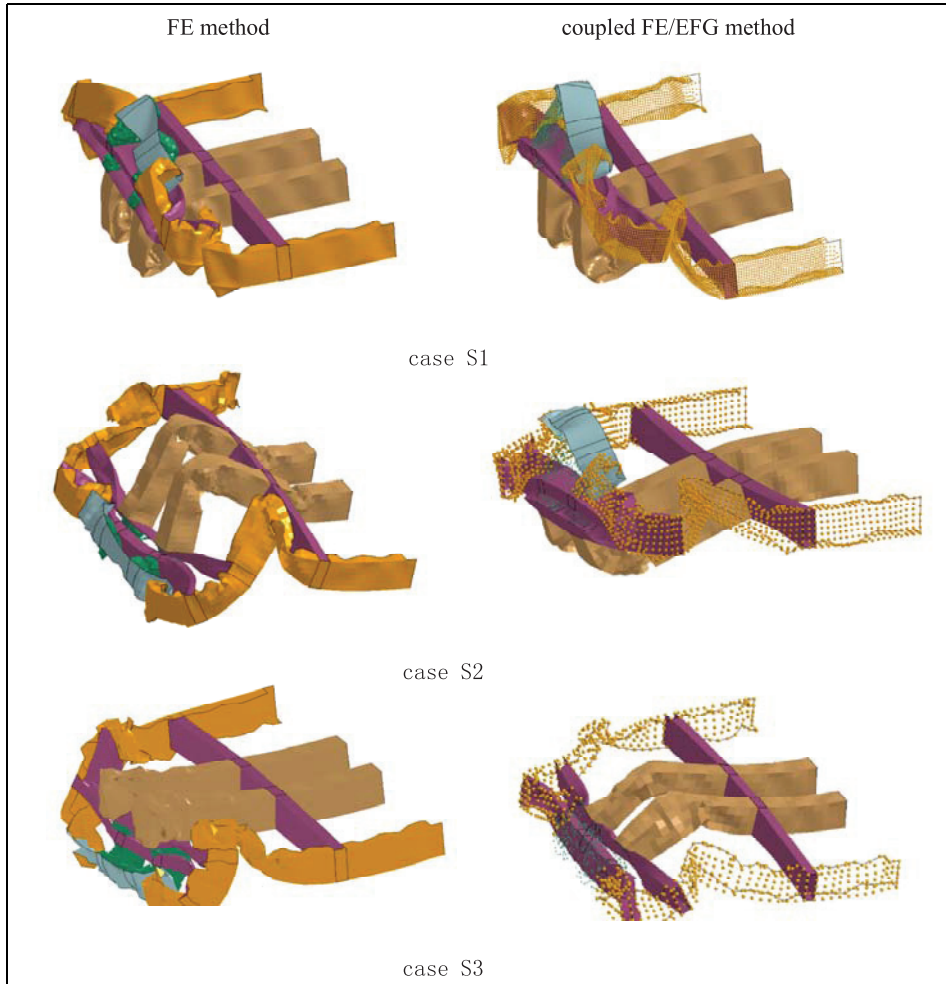


**Figure 10.** Underframe deformation.

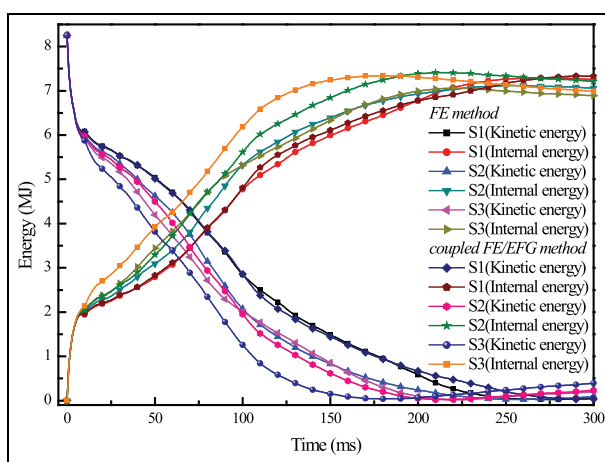


**Figure 11.** Time series of energy.

mesh model can capture smaller deformation and converts the kinetic energy into internal energy at a slower rate, while the mesh model with higher density produces more significant deformation, dissipating the kinetic

energy more rapidly. As shown in Figure 12, the comparison between deformations for case S1 and case S3 at  $t = 85\text{ ms}$  also proves that coarse mesh models produce relatively severe deformation.

To further study the sensitivity of mesh density variation, we use variance function to quantitatively estimate the influence of mesh density on time series of kinetic energy, internal energy and the reaction force of the rigid wall. The variance function can be written as follows

$$D_{X_s}(t) = E \left\{ [X_s(t) - \bar{X}_s(t)]^2 \right\} \quad (6)$$

where  $X_s(t)$  is the time series data;  $\bar{X}_s(t)$  is the mean function which can be written as follows

$$\bar{X}_s(t) = \frac{1}{n} \sum_{s=1}^n X_s(t) \quad (7)$$

where  $n$  is the length of time series data  $X_s(t)$ . According to equation (6), the variance functions of

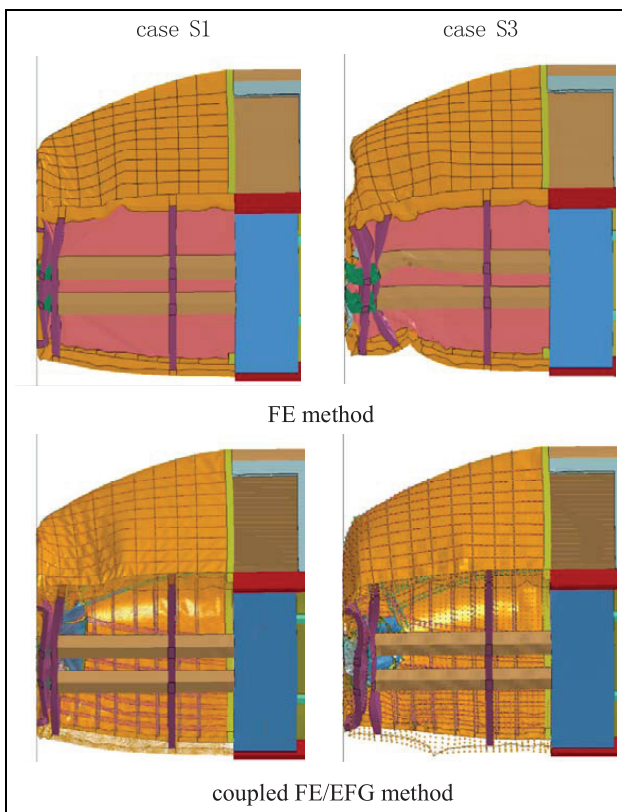


**Figure 12.** Deformations of case S1 and case S3 at  $t = 85$  ms.

kinetic energy and internal energy are shown in Figure 13.

The two plots show that the variance of the coupled FEM/EFGM is larger than the variance of the FEM, which means that the coupled FEM/EFGM is more sensitive to the mesh density than the FEM in terms of kinetic energy and internal energy. The time series of force for both methods under different levels of mesh density are plotted in Figure 14.

In Figure 14, there are two peaks in the main stage of the collision simulation, respectively, corresponding to the moment when the energy absorption tube and the draft sill in front of the train begin to deform during the collision. It can be seen that the two peak values of the two methods increased with the increasing in the mesh size, but the increments of coupled FEM/EFGM is larger than that of FEM. Besides, some irrational oscillation waveforms are also appeared, which shows that the models of two methods are easy to become unstable in the simulation with the increase in the mesh size. The variance function of reaction force of the rigid wall is shown in Figure 15.

Therefore, we further calculate the sum of the two variance function of the coupled FEM/EFGM and FEM over the time. They are 245.815 and 121.24, respectively. Comparing the sum, we find that coupled FEM/EFGM is also more sensitive to mesh density than FEM in terms of reaction force. So, it is can be concluded that mesh density affects simulation results of both FEM and coupled FEM/EFGM and specifically has more significant influences over the coupled FEM/EFGM than the FEM.

**Hourglass energy.** Hourglass is an important indicator to measure the reliability of a crash simulation result. The relationships between hourglass energy variation with respect to time of FEM and coupled FEM/EFGM are plotted in Figure 16.

In Figure 16, hourglass energy increases with time and mesh density. More specifically, the hourglass energy increases rapidly during the initial stage of the crash and eventually converges to a stable level or increases at a steadily slow pace towards the end of the crash. The hourglass energy percentage is shown in Figure 17. In the FEM, the hourglass in the three cases are 2.06%, 4.64% and 7.54%, respectively, while in

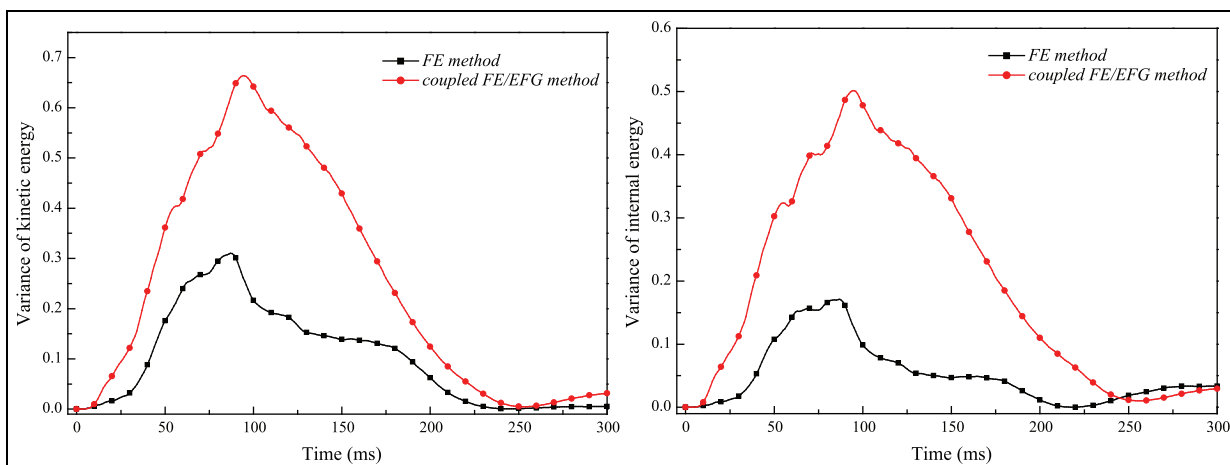


**Figure 13.** Variance function of kinetic energy and internal energy.

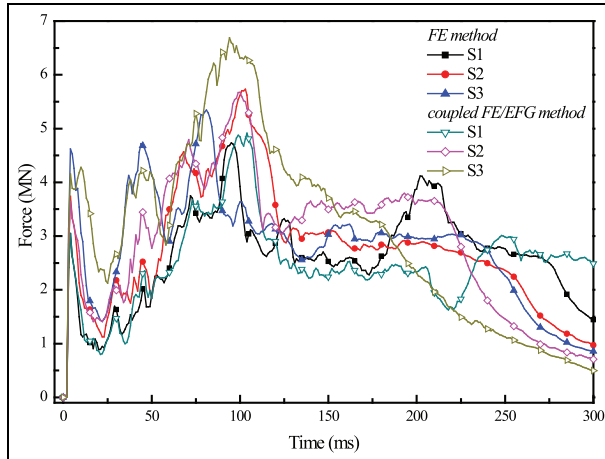


**Figure 14.** Time series of force.

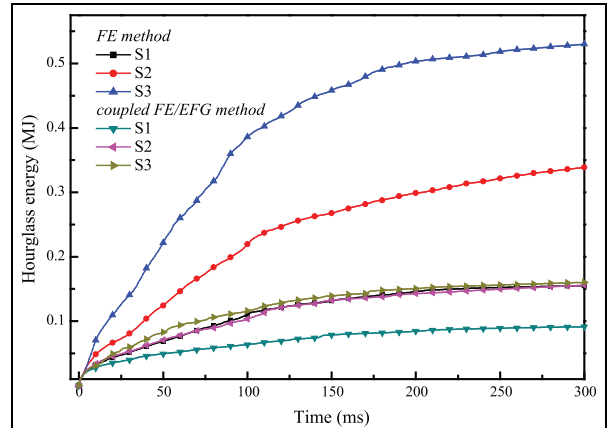


**Figure 16.** Relationship of hourglass energy with respect to time.

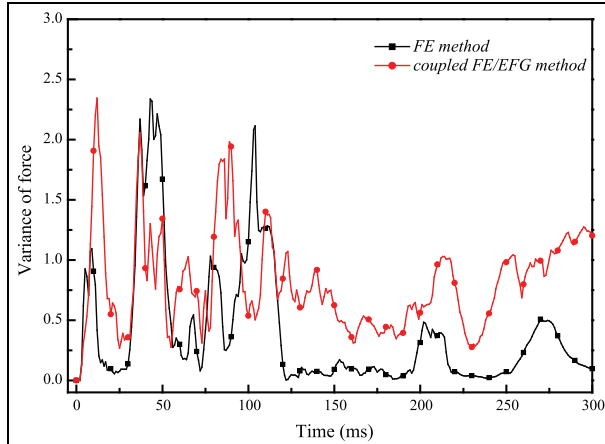


**Figure 15.** Variance function of reaction force of rigid wall.

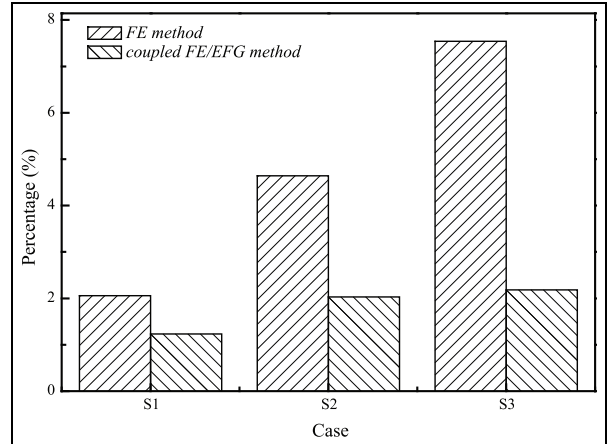


**Figure 17.** Comparison of hourglass energy percentage of hourglass energy.

coupled FEM/EFGM, they are 1.23%, 2.03% and 2.18%, respectively. It is clear that the hourglass energy percentage of coupled FEM/EFGM is much smaller than FEM.

As previously mentioned, FE analysis of crash simulation often encounters the problem of hourglass control. Some solutions, such as using hourglass stabilized elements or full integration, do not always work in practical problems. For example, the implementation of full integration is time-consuming and it may also introduce shear locking phenomenon.<sup>21</sup> Obviously, coupled FEM/EFGM outperforms the conventional FEM in hourglass control, thus providing an alternative method for hourglass control in railway vehicle crashworthiness simulation.

## Conclusion and future work

In this article, we introduce a coupled FEM/EFGM to rail vehicle crashworthiness simulation. A full-scale

simulation of crashworthiness analysis has been conducted to demonstrate its potential usage in railway industry. Comparisons between the conventional FEM and the novel coupled method are based on the simulation results from different levels of mesh density. The main conclusions of this research and some suggestions are listed as follows:

1. The coupled FEM/EFGM is a suitable alternative for full-size rail vehicle crashworthiness simulation by reasonably simplifying the structure of the vehicle and applying EFGM to those components undergoing large nonlinear deformation.
2. With a modelling strategy to allocate EFG model to largely deformed component, the coupled FEM/EFGM can provide acceptable computational efficiency and high simulation accuracy. However, compared to FEM, the

- computation time and memory consumption of coupled FEM/EFGM are more sensitive to mesh density of models. Therefore, care should be taken by users when increasing the mesh density in coupled FEM/EFGM so that it does not lead to unacceptable computation time and memory consumption.
3. The coupled method can use a relatively coarse mesh model to produce an accurate simulation. It shows that we can use coarser mesh model in the coupled method than in the conventional FEM to reduce the computation time but retain the simulation accuracy.
  4. The coupled FEM/EFGM has advantage in hourglass energy control over the conventional FEM, which provides an effective way of reducing hourglass energy at lower mesh density in crashworthiness simulation.

In the future, it is anticipated that the coupled FEM/EFGM will attract more interest in rail vehicle crashworthiness analysis with the advances in computing power.

### Declaration of conflicting interests

The author(s) declared no potential conflicts of interest with respect to the research, authorship, and/or publication of this article.

### Funding

The author(s) disclosed receipt of the following financial support for the research, authorship, and/or publication of this article: This research was supported by National Natural Science Foundation of China (51405402, 51475394) and the Self-developed Research Project of the State Key Lab of Traction Power (2015TPL\_T06).

### References

1. Pereira MS. Structural crashworthiness of railway vehicles. In: *7th world congress of rail research*, Montreal, QC, Canada, 2006, <http://www.railway-research.org/IMG/pdf/183-2.pdf>
2. Jacobsen K, Tyrell D and Perlman B. Impact test of a crash-energy management passenger rail car. In: *ASME/IEEE 2004 joint rail conference*, Baltimore, MD, 6–8 April 2004, pp.19–26. New York: IEEE.
3. Tyrell D, Jacobsen K, Martinez E, et al. Train-to-train impact test of crash energy management passenger rail equipment: structural results. In: *ASME 2006 international mechanical engineering congress and exposition*, Chicago, IL, 5–10 November 2006, pp.35–44. New York: American Society of Mechanical Engineers (ASME).
4. Jacobsen K, Tyrell D and Perlman B. Impact tests of crash energy management passenger rail cars: analysis and structural measurements. In: *ASME 2004 international mechanical engineering congress and exposition*, Anaheim, CA, 13–19 November 2004, pp.97–105. New York: American Society of Mechanical Engineers (ASME).
5. Li R, Xu P, Peng Y, et al. Scaled tests and numerical simulations of rail vehicle collisions for various train sets. *Proc IMechE Part F: J Rail and Rapid Transit*. Epub ahead of print 16 September 2015. DOI: 10.1177/0954409715605126.
6. Afazov S, Denmark W and Yaghi A. Modelling aspects of the design of railway vehicle structures and their crashworthiness. *Proc IMechE Part F: J Rail and Rapid Transit*. Epub ahead of print 18 September 2015. DOI: 10.1177/0954409715605141.
7. Xue X, Robinson M, Schmid F, et al. Rail vehicle impact analysis: a critique of the suitability of the rigid wall model and the assumption of symmetrical behaviour. *Proc IMechE Part F: J Rail and Rapid Transit* 2015; 229: 173–185.
8. Montalbán L, Real J and Real T. Mechanical characterization of railway structures based on vertical stiffness analysis and railway substructure stress state. *Proc IMechE Part F: J Rail and Rapid Transit* 2013; 227: 74–85.
9. Wang H-P, Botkin ME, Wu C-T, et al. Coupled finite element/meshfree simulation of manufacturing problems. In: *ASME 2003 pressure vessels and piping conference*, Cleveland, OH, 20–24 July 2003, pp.195–200. New York: American Society of Mechanical Engineers (ASME).
10. Ibrahim HK. *Design optimization of vehicle structures for crashworthiness improvement*. Montreal, QC, Canada: Concordia University, 2009.
11. R. No. 66: Uniform technical prescriptions concerning the approval of large passenger vehicles with regard to the strength of their superstructure. In: *World Forum for Harmonization of Vehicle Regulations (WP. 29)*, 2006, <http://www.unece.org/fileadmin/DAM/trans/main/wp29/wp29regs/r066r1e.pdf>
12. Baykasoglu C, Mugan A, Sunbuloglu E, et al. Rollover crashworthiness analysis of a railroad passenger car. *Int J Crashworthiness* 2013; 18: 492–501.
13. Liu G-R. *Meshfree methods: moving beyond the finite element method*. Boca Raton, FL: Taylor & Francis, 2009.
14. Belytschko T, Organ D and Krongauz Y. A coupled finite element-element-free Galerkin method. *Comput Mech* 1995; 17: 186–195.
15. Wang H-P, Pan Y-C and Cheng Y-P. Crashworthiness simulation using coupled meshfree/finite element formulations in LS-DYNA. In: *9th international LS-DYNA® users conference*, Dearborn, MI, 4–6 June 2006, <http://www.dynalook.com/international-conf-2006/41CrashSafety.pdf>
16. Wang H-P, Wu C-T, Guo Y, et al. A coupled meshfree/finite element method for automotive crashworthiness simulations. *Int J Impact Eng* 2009; 36: 1210–1222.
17. Jang H-J, Shin K-B and Han S-H. Numerical study on crashworthiness assessment and improvement of composite carbody structures of tilting train using hybrid finite element model. *Adv Compos Mater* 2012; 21: 371–388.
18. Kambur C. *Assessment of mesh-free methods in LS-DYNA: modeling of barriers in crash simulation*. MSc

- Thesis, Institute for Structural Mechanics, Stuttgart, 2004.
19. Dvorkin EN and Bathe K-J. A continuum mechanics based four-node shell element for general non-linear analysis. *Eng Computation* 1984; 1: 77–88.
20. Lu Y, Belytschko T and Gu L. A new implementation of the element free Galerkin method. *Comput Method Appl M* 1994; 113: 397–414.
21. Hallquist JO. *LS-DYNA® keyword user's manual, vol. II: material models*. Livermore, CA: Livermore Software Technology Corporation (LSTC), 2013.